Supporting Information for

Efficient Electrochemical CO_2 Conversion Powered by Renewable Energy

Douglas R. Kauffman,[1,*] Jay Thakkar,[1] Rajan Siva,[1] Christopher Matranga,[1] Paul R. Ohodnicki,[1] Chenjie Zeng[2] and Rongchao Jin[2]

[1]National Energy Technology Laboratory, United States Department of Energy, Pittsburgh, Pennsylvania, USA. *Email: Douglas.Kauffman@NETL.DOE.GOV

[2]Dept. of Chemistry, Carnegie Mellon University, Pittsburgh, Pennsylvania, USA

Contents Pages

Experimental Section

General. $Au_{25}(C_2H_4Ph)_{18}$ nanoclusters were synthesized following previously published methods.[1,2] Absorbance spectroscopy was conducted on an Agilent 8453 diode array spectrophotometer. All electrochemical experiments were conducted in 0.1M $KHCO_3$ using a Ag/AgCl reference electrode and a Pt mesh counter electrode. The Ag/AgCl reference electrode was regularly calibrated against a Hydroflex reversible hydrogen electrode in CO_2 saturated 0.1M $KHCO_3$. Purified water (17-18 MΩ, Barnstead Easypure) was used to prepare all aqueous solutions and to clean all glassware. A Basi Epsilon potentiostat was used for potentiostat-controlled experiments. A 6V, 1.5W solar panel (RadioShack; model 2770052) was used for solar cell-powered experiments. A rechargeable 6V battery (Universal Power Group; model UB645k) was charged with a 6V solar charger (American Hunter; Model BL-66-S) and used for battery-powered experiments.

Electrode Preparation. A small amount of Au_{25} was dissolved in 3 mL acetone and the UV-Vis absorbance spectrum was collected in a 1 cm quartz cuvette. The concentration of Au_{25} (mol L^{-1}) was determined using the known molar absorptivity at 670 nm (8800 L mol^{-1} cm^{-1}).[3] Specific electrode loadings were obtained by mixing precise volumes of Au_{25} solution with 2 mg of carbon black (CB) dispersed in 2 mL methanol. The mixture was sonicated for approximately 1 minute to ensure complete mixing. Au_{25} is not soluble in methanol and this process precipitates Au_{25} onto the CB support. The mixture was diluted with ultrapure water and centrifuged twice to remove the methanol. The centrifuged Au_{25}/CB material was dried under N_2 and then suspended in 2 ml H_2O by adding 75 µl Nafion solution and sonicating. The resulting Au_{25}/CB suspension was dropcast onto 25 cm^2 carbon paper electrodes heated at 135 C. This temperature was high

enough to evaporate water but lower than the ~200 C required for ligand desorption.[4] The Au_{25}/CB material occupied approximately 13 cm^2 of the electrode surface, and the edges of the carbon paper electrodes remained bare.

Reactor Design and Operation. A continuous flow, glass reactor was used to study the electrocatalytic reduction of CO_2. The reactor was an H-cell design constructed from two 150 mL chambers (Addams & Chittenden Scientific Glassware; microbial fuel cell model 100.25.3). The cathode chamber contained the Au_{25}/CB coated carbon paper electrode and a Ag/AgCl reference electrode. The anode half-cell compartment contained the platinum mesh counter electrode. The two chambers were separated by a 0.007 inch thick Nafion 117 cation exchange membrane. Ultrahigh purity CO_2 (UHP; 99.999%) was continuously purged at a constant rate through the cathode compartment electrolyte. A constant potential was applied to the cathode with a potentiostat, solar cell or solar-rechargeable battery. The effluent gas was collected in a gas-tight 1 liter Tedlar bag (Supelco) and products were quantified using a Perkin Elmer Arnel Clarus 600 gas chromatograph (GC). The GC was equipped with a 15' x 1/8" (2.1 mm inner diameter) Supelco 60/80 Carboxen 1000 column. The GC was calibrated with a multi-component standard gas mixture containing certified concentrations of H_2, N_2, O_2, CO, CO_2, and CH_4. The mixture was balanced with He. Each calibration point was conducted in triplicate to ensure reproducibility. The column can also detect other common CO_2 reduction products including acetylene, ethane, ethylene and methanol, but we only detected CO and H_2. Faradaic efficiency calculations show that the detected products (CO and H_2) account for ~100% of the electrochemical current, which provides further evidence that our product analysis is accurate. These result is consistent with previous work by our group and others that Au species selectivity

convert CO_2 into CO.[5-9] The anode compartment electrolyte was purged with N_2 and continuously exchanged from a larger 1 liter reservoir with peristaltic pumps.

Faradaic Efficiency. Faradaic efficiency (FE) estimates the fraction of electrons used in the CO_2RR. Ideally, all electrons passed through the electrode are used in the CO_2RR reaction and the system shows 100% FE. FE values were calculated from the detected reaction products and the integrated electrolysis charge. In a continuous flow reactor the amount of products contained in the effluent gas *per* unit time can be determined from the flow rate, sampling time, and GC injection volume. For example, we collected 500 mL of effluent gas in a sampling bag every 10 minutes (50 mL min^{-1} flow rate). We injected 0.5 mL of this gas into the GC to quantify the amount of products. The GC injection volume was $1/1000^{th}$ the sample volume, so the detected products represented $1/1000^{th}$ the total amount of gas produced during the 10 min sampling period. Faradaic efficiencies were then determined from the amount of charge passed during the sampling period. FE values for multi-hour and multi-day runs were calculated from the average daily charge per minute passing through the cathode.

Equation S1. Faradaic Efficiency Calculation.

$$\mathrm{FE}\ (\%) = \frac{\text{Detected Products (mol CO)} \times \frac{2\ \text{mol e}^-}{\text{mol CO}}}{\frac{\text{Electrolysis Charge (C)}}{96485\ \frac{\text{C}}{\text{mol e}^-}}} = \frac{\text{mol e}^-\text{consumed by products}}{\text{mol e}^-\ \text{passed through electrode}}$$

Calculating the electrical input required for CO_2 Conversion. The electrical input (MWh) that is required to convert one metric tonne (1000 kg) of CO_2 into CO (or any other product) can be calculated as follows:

Equation S2. One metric tonne (1000 kg) CO_2 is equal to 22727.3 mol CO_2.

$$1 \text{ tonne } CO_2 \left(\frac{1000 \text{ kg}}{\text{tonne}}\right)\left(\frac{\text{mol } CO_2}{0.044 \text{ kg}}\right) = 22727.3 \text{ mol } CO_2$$

Equation S3. 4.3857×10^9 Coulombs of charge are required to convert 22727.3 mol CO_2 into CO (2 e^- process) assuming 100% Faradaic efficiency (FE).

$$22727.3 \text{ mol } CO_2 \left(\frac{2 \text{ e}^-}{CO_2}\right)\left(\frac{96485 \text{ C}}{\text{mol e}^-}\right)\left(\frac{1}{100\% \text{ FE}}\right) = 4.3857 \times 10^9 \text{ C}$$

Equation S4. 3600 C are equivalent to 1 ampere hour (Ah).

$$4.3857 \times 10^9 \text{C} \left(\frac{\text{A} \cdot \text{s}}{\text{C}}\right)\left(\frac{\text{h}}{3600\text{s}}\right) = 1.2182 \times 10^6 \text{Ah}$$

Equation S5. Electricity is typically reported in units of watt hours (W = A·V). The formal potentials for CO formation and water oxidation are –0.106V and +1.23 V *vs* RHE, respectively. At zero overpotential (η=0V) the total cell voltage would be 1.336 V and it would require 1.628 MWh of electricity to convert one tonne of CO_2 into CO. Energy requirements for additional products and non-ideal, real-world systems are summarized in tables S1 and S2.

$$1.2182 \times 10^6 \text{Ah} * 1.336 \text{ V} \left(\frac{\text{W}}{\text{A} \cdot \text{V}}\right) = 1.628 \text{ MWh}$$

Table S1. Ideal Energy requirements (MWh/tonne CO_2) for converting CO_2 into various products at zero overpotential and 100% Faradaic efficiency (FE). Values were calculated using equations S1-S4.

Product	ne^-	FE (%)	Cathode Voltage (V vs. RHE)	Anode Voltage (V vs. RHE)	Total Cell Voltage (V)	Overpotential "η" (V)	MWh / tonne CO_2
CO	2	100	-0.106	1.23	1.34	0	1.628
HCOOH	2	100	-0.250	1.23	1.41	0	1.803
HCHO	4	100	-0.070	1.23	1.38	0	3.167
CH_3OH	6	100	0.016	1.23	1.23	0	4.437
CH_4	8	100	0.169	1.23	1.06	0	5.170
C_2H_4	12	100	0.064	1.23	1.16	0	8.523

Table S2. Energy requirements (MWh/tonne CO_2) for selected catalyst systems to convert one tonne CO_2 in to various products. We assumed 500 mV overpotential for anodic OER and all voltages are in the RHE scale.

Sample	Product	FE	Cathode Voltage	Anode Voltage	Cell Voltage	MWh / tonne CO_2	Ref.
Au_{25}	CO	0.99	-1	1.73	2.73	3.36	5,6
Au_{25}	CO	0.87	-1	1.73	2.73	3.82	*This work*
4nm Au NP	CO	0.90	-0.9	1.73	2.63	5.17	7
6 nm Au NP	CO	0.71	-0.9	1.73	2.63	4.51	7
8 nm Au NP	CO	0.71	-0.9	1.73	2.63	4.51	7
10 nm Au NP	CO	0.89	-0.9	1.73	2.63	3.60	7
Au NWs	CO	0.9	-0.55	1.73	2.28	3.09	8
Au-oxide NPs	CO	0.99	-0.5	1.73	2.23	2.74	9
CuOx NPs	CO	0.61	-1.0	1.73	2.43	5.45	10
Ag	CO	0.99	n/a	n/a	2.5	3.08	11
Ag/CN	CO	0.90	-1.15	1.73	2.88	3.90	12
Bulk CuOx	CO + HCOOH	0.69	-0.5	1.73	2.23	3.94	13
SnO_2	CO + HCOOH	0.99	-0.7	1.73	2.43	2.99	14
PbO_2	HCOOH	1	-0.75	1.73	2.48	3.02	15
5nm SnO_2 NPs	HCOOH	0.86	-1.6	1.73	3.33	4.72	16
PEI-NCNT	HCOOH	.85	-1.19	1.73	2.92	4.19	17
Boron-doped diamond	HCOH	0.62	-0.877	1.73	2.607	10.25	18
RuO_2	CH_3OH	0.6	-0.6	1.73	2.33	14.19	19
Cu-oxide	CH_3OH	0.38	-0.5	1.73	2.23	21.45	20
Mo	CH_3OH	0.5	-0.364	1.73	2.094	15.31	20
RuO_2-TiO_2	CH_3OH	0.46	-0.364	1.73	2.094	16.64	20
Cu	CH_4	0.723	-1.05	1.73	2.78	18.74	21
Cu NPs	CH_4	0.77	-1.35	1.73	3.08	19.49	22
Bulk Cu	C_2H_4	0.481	-1.052	1.73	2.782	42.28	20
Bulk Cu	C_2H_4	0.5	-0.927	1.73	2.657	38.84	23

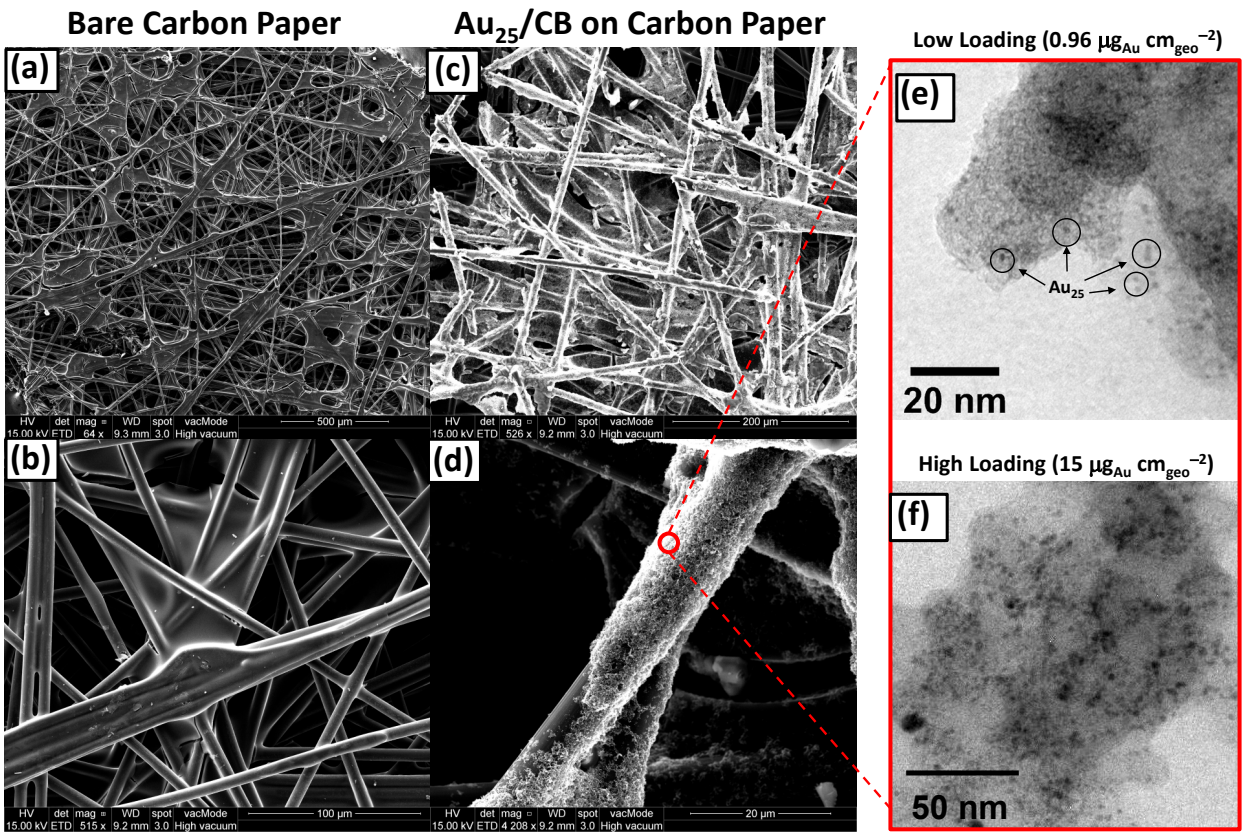

Figure S1. Scanning electron microscope images of (a,b) a bare carbon paper electrode and (c,d) Au_{25}/CB deposited onto a carbon paper electrode. (e,f) Transmission electron microscope (TEM) images showing well dispersed 1.4±0.4 nm Au_{25} particles in the low loading regime (0.96 μg_{Au} cm^{-2}) and aggregated Au_{25} particles in the high and loading regime (15 μg_{Au} cm^{-2}). Au_{25}/CB samples were scraped from the surface of the electrode, sonicated in methanol, and then deposited onto lacey carbon grids for TEM imaging.

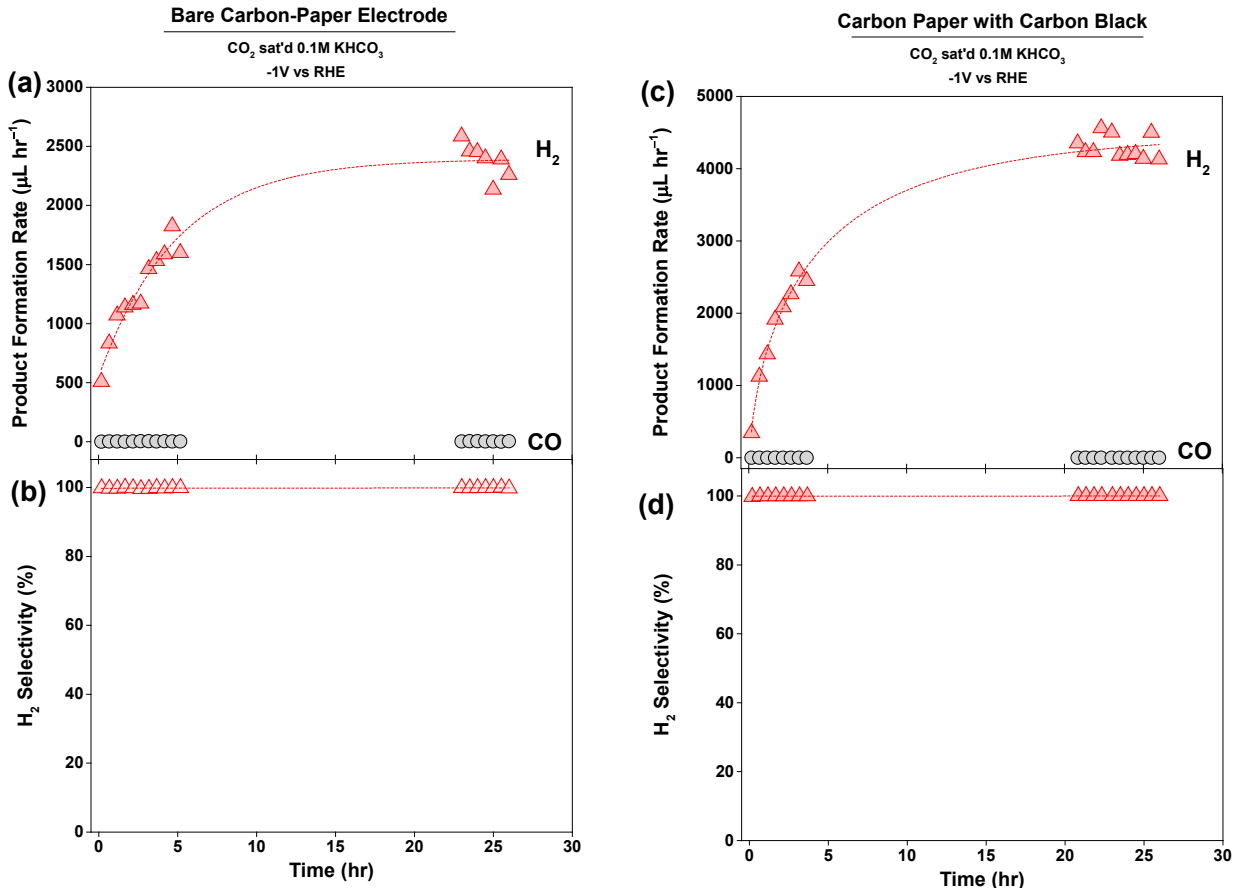

Figure S2. Product formation rates (μL hr^{-1}) and H_2 selectivity for (a,b) a bare carbon paper electrode (99.8 ± 0.1% H_2 selectivity) and (c,d) carbon black on carbon paper electrode (99.95 ± 0.06% H_2 selectivity) operated at −1V *vs*. RHE in 0.1M $KHCO_3$ bubbled with CO_2 at 50 mL min^{-1}. Both electrodes showed selective H_2 evolution that increased over time; dashed lines serve as a guide for the eye. Increased H_2 evolution over time likely stems from the electrolyte slowly wetting the finely woven carbon paper electrode.

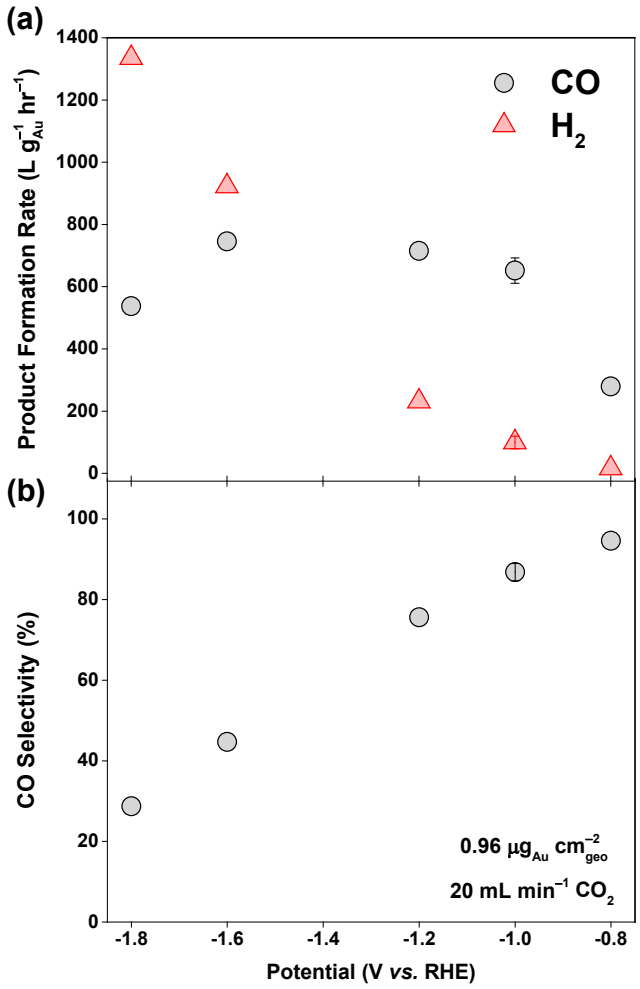

Figure S3. (a) Product formation rates and (b) CO selectivity for an Au_{25}-containing electrode as a function of applied potential in CO_2 saturated 0.1M $KHCO_3$. Catalyst loading was 0.96 μg_{Au} cm_{geo}^{-2} and the CO_2 flow rate was 20 mL min^{-1}.

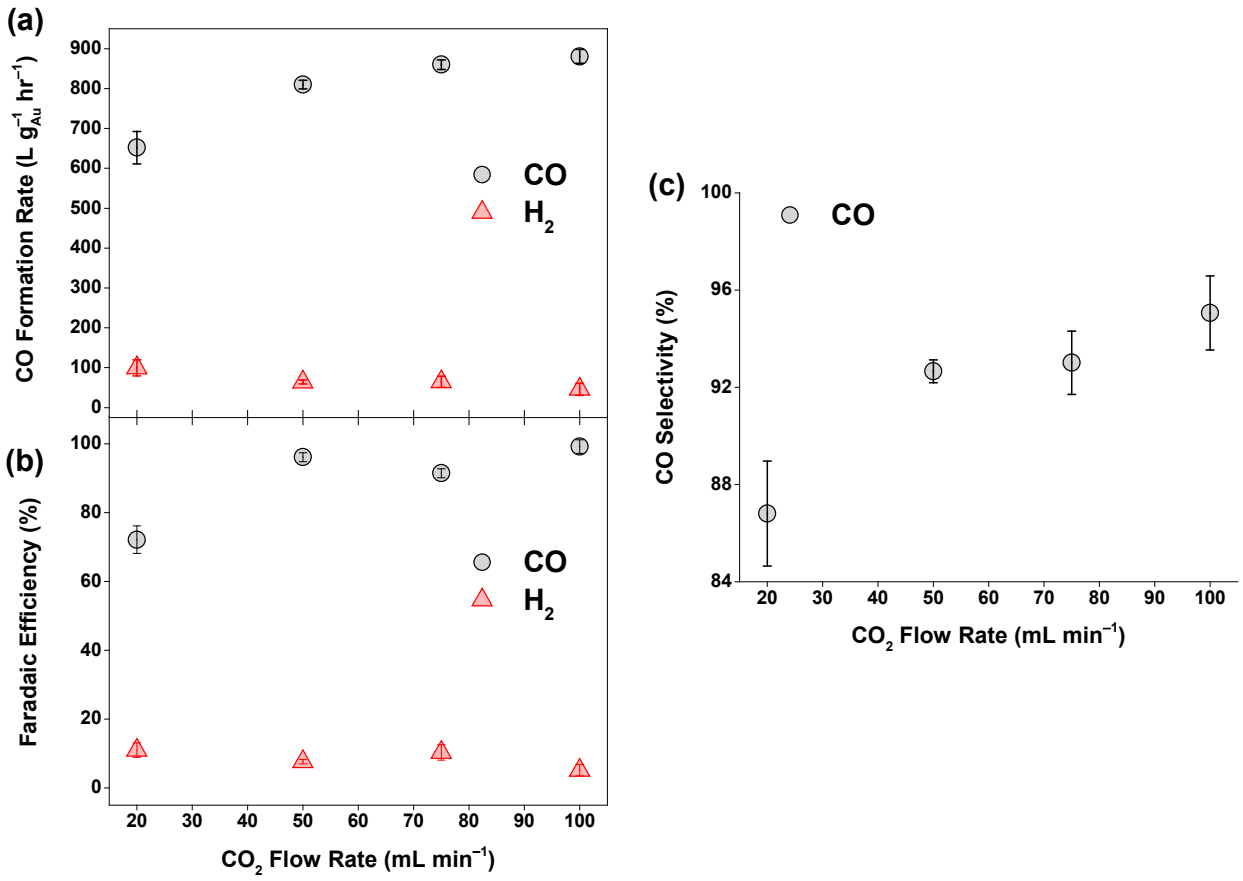

Figure S4. (a) Product formation rates, (b) Faradaic efficiency and (c) CO selectivity as a function of CO_2 flow rate (mL min^{-1}) in 0.1M $KHCO_3$. Catalyst loading was 0.96 μg_{Au} cm_{geo}^{-2} and the cathode potential was −1V *vs*. RHE.

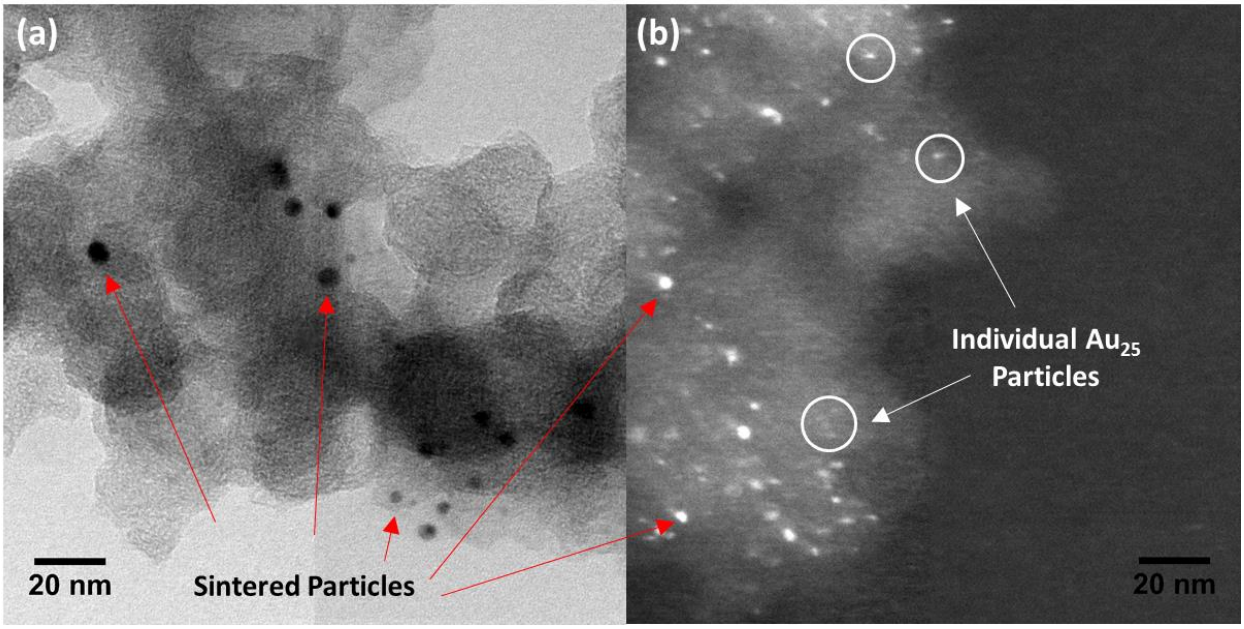

Figure S5. (a) Brightfield and (b) darkfield TEM images of Au_{25}/CB after 36 hours of CO_2 electrolysis at −1V vs RHE. The TEM images show larger sintered particles and some individual Au_{25} particles after 36 hours of electrolysis. White circles highlight some of the individual Au_{25} particles in panel b.

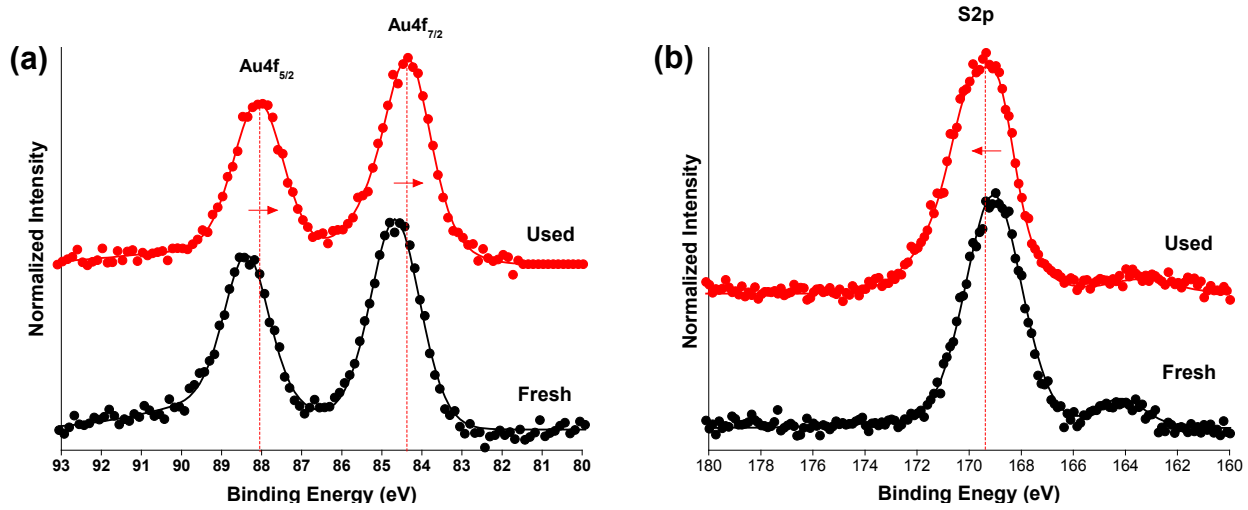

Figure S6. X-ray photoelectron spectroscopy (XPS) of the Au4f (a) and S2p (b) spectral regions before (black) and after (red) 36 hours of CO_2 electrolysis.

A downshift in the Au_{4f} binding energy combined with an upshift in S2p binding energy suggests some particle sintering and/or thiolate desorption from the Au_{25} nanocluster after extended electrolysis. Specifically, desorption of the electron-withdrawing ligands should return some electron density to the Au nanocluster and induce a downshift in Au 4f binding energy. Furthermore, desorption of thiol groups from Au surfaces produces an upshift in S2p binding energy.[24] Ligand desorption can lead to particle sintering, which provides an explanation for the increased post-reaction particle sizes shown in Figure S5.

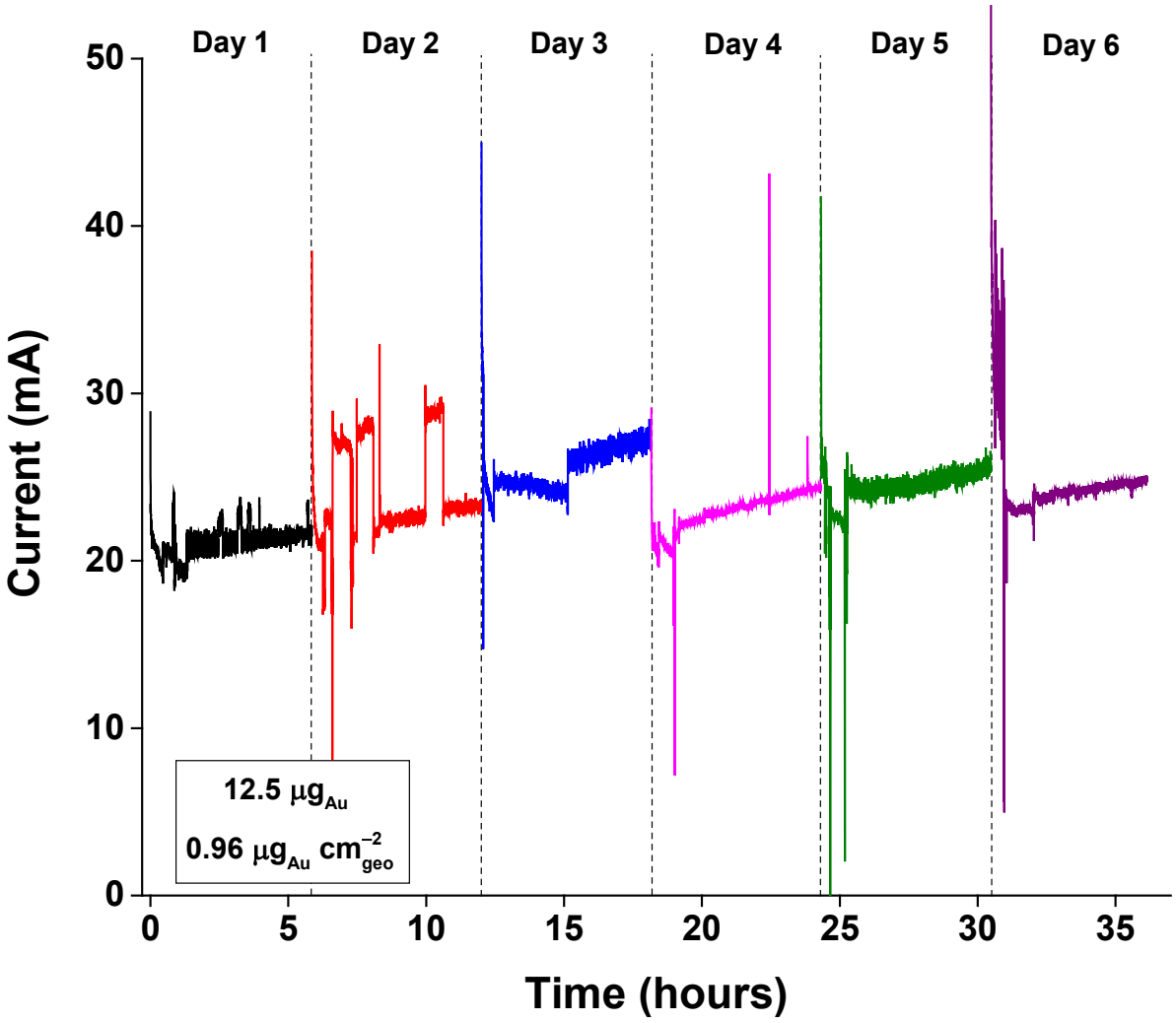

Figure S7. Day-to-day CO_2RR current in 0.1M $KHCO_3$ bubbled with CO_2 at 50 mL min^{-1}. The electrode was operated at −1V vs RHE and it contained 0.96 μg_{Au} cm_{geo}^{-2} (12.5 μg total Au loading).

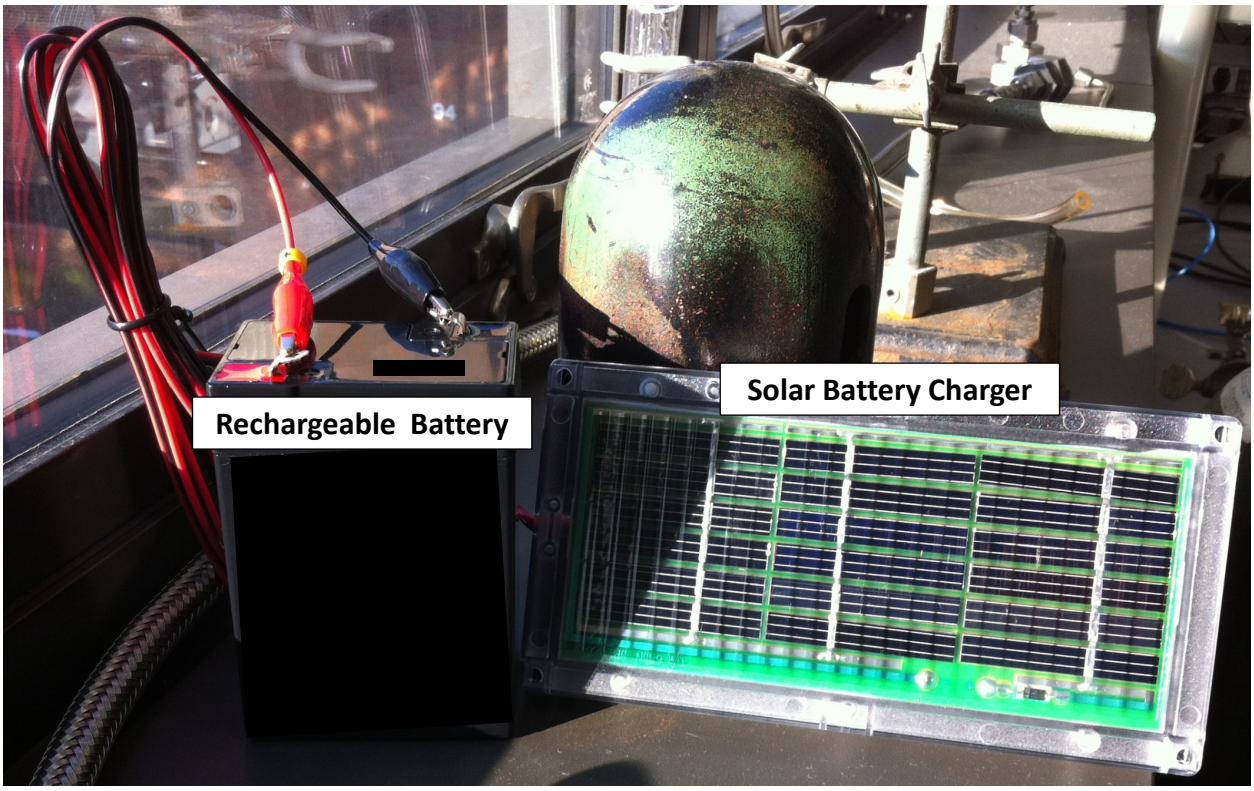

Figure S8. Photograph of solar-rechargeable battery.

REFERENCES

1. Zhu, M.; Aikens, C. M.; Hollander, F. J.; Schatz, G. C.; Jin, R. Correlating the Crystal Structure of a Thiol-Protected Au_{25} Cluster and Optical Properties. *J. Am. Chem. Soc.* **2008**, *130*, 5883-5885.

2. Heaven, M. W.; Dass, A.; White, P. S.; Holt, K. M.; Murray, R. W. Crystal Structure of the Gold Nanoparticle $[N(C_8H_{17})_4][Au_{25}(SCH_2CH_2Ph)_{18}]$. *J. Am. Chem. Soc.* **2008**, *130*, 3754-3755.

3. Negishi, Y.; Nobusada, K.; Tsukuda, T. Glutathione-Protected Gold Clusters Revisited: Bridging the Gap between Gold(I)−Thiolate Complexes and Thiolate-Protected Gold Nanocrystals. *J. Am. Chem. Soc.* **2005**, *127*, 5261-5270.

4. Nie, X.; Qian, H.; Ge, Q.; Xu, H.; Jin, R. CO Oxidation Catalyzed by Oxide-Supported $Au_{25}(SR)_{18}$ Nanoclusters and Identification of Perimeter Sites as Active Centers. *ACS Nano* **2012**, *6*, 6014-6022.

5. Kauffman, D. R.; Alfonso, D.; Matranga, C.; Ohodnicki, P.; Deng, X.; Siva, R. C.; Zeng, C.; Jin, R. Probing active site chemistry with differently charged Au_{25}^q nanoclusters (q = −1, 0, +1). *Chem. Sci.* **2014**, *5*, 3151-3157.

6. Kauffman, D. R.; Alfonso, D.; Matranga, C.; Qian, H.; Jin, R. Experimental and Computational Investigation of Au_{25} Clusters and CO_2 : A Unique Interaction and Enhanced Electrocatalytic Activity. *J. Am. Chem. Soc.* **2012**, *134*, 10237-10243.

7. Zhu, W.; Michalsky, R.; Metin, O. n.; Lv, H.; Guo, S.; Wright, C. J.; Sun, X.; Peterson, A. A.; Sun, S. Monodisperse Au Nanoparticles for Selective Electrocatalytic Reduction of CO_2 to CO. *J. Am. Chem. Soc.* **2013**, *135*, 16833-16836.

8. Zhu, W.; Zhang, Y.-J.; Zhang, H.; Lv, H.; Li, Q.; Michalsky, R.; Peterson, A. A.; Sun, S. Active and Selective Conversion of CO_2 to CO on Ultrathin Au Nanowires. *J. Am. Chem. Soc.* **2014**, *136*, 16132-16135.

9. Chen, Y.; Li, C. W.; Kanan, M. W. Aqueous CO_2 Reduction at Very Low Overpotential on Oxide-Derived Au Nanoparticles. *J. Am. Chem. Soc.* **2012**, *134*, 19969-19972.

10. Kauffman, D. R.; Ohodnicki, P. R.; Kail, B. W.; Matranga, C. Selective Electrocatalytic Activity of Ligand Stabilized Copper Oxide Nanoparticles.pdf. *J. Phys. Chem. Lett.* **2011**, *2*, 2038-2043.

11. Rosen, B. A.; Salehi-Khojin, A.; Thorson, M. R.; Zhu, W.; Whipple, D. T.; Kenis, P. J. A.; Masel, R. I. Ionic Liquid-Mediated Selective Conversion of CO_2 to CO at Low Potentials. *Science* **2011**, *334*, 643-644.

R.; Ma, S.; Gewirth, A. A.; Kenis, P. J. A. Nitrogen-Based Catalysts for the Electrochemical Reduction of CO_2 to CO. *J. Am. Chem. Soc.* **2012**, *134*, 19520-19523.

13. Li, C. W.; Kanan, M. W. CO_2 Reduction at Low Overpotential on Cu Electrodes Resulting from the Reduction of Thick Cu_2O Films. *J. Am. Chem. Soc.* **2012**, *134*, 7231-7234.

14. Chen, Y.; Kanan, M. W. Tin Oxide Dependence of the CO2 Reduction Efficiency on Tin Electrodes and Enhanced Activity for Tin/Tin Oxide Thin-Film Catalysts. *J. Am. Chem. Soc.* **2012**, *134*, 1986-1989.

15. Lee, C. H.; Kanan, M. W. Controlling H^+ *vs* CO_2 Reduction Selectivity on Pb Electrodes. *ACS Catal.* **2014**, *5*, 465-469.

16. Zhang, S.; Kang, P.; Meyer, T. J. Nanostructured Tin Catalysts for Selective Electrochemical Reduction of Carbon Dioxide to Formate. *J. Am. Chem. Soc.* **2014**, *136*, 1734-1737.

17. Zhang, S.; Kang, P.; Ubnoske, S.; Brennaman, M. K.; Song, N.; House, R. L.; Glass, J. T.; Meyer, T. J. Polyethylenimine-Enhanced Electrocatalytic Reduction of CO_2 to Formate at Nitrogen-Doped Carbon Nanomaterials. *J. Am. Chem. Soc.* **2014**, *136*, 7845-7848.

18. Nakata, K.; Ozaki, T.; Terashima, C.; Fujishima, A.; Einaga, Y. High-Yield Electrochemical Production of Formaldehyde from CO_2 and Seawater. *Angew. Chem. Int. Ed.* **2014**, *53*, 871-874.

19. Herron, J. A.; Kim, J.; Upadhye, A. A.; Huber, G. W.; Maravelias, C. T. A general framework for the assessment of solar fuel technologies. *Energy Environ. Sci.* **2015**, *8*, 126-157.

20. Qiao, J.; Liu, Y.; Hong, F.; Zhang, J. A Review of Catalysts for the Electroreduction of Carbon Dioxide to Produce Low-Carbon Fuels. *Chem. Soc. Rev.* **2014**, *43*, 631-675.

21. Peterson, A. A.; Nørskov, J. K. Activity Descriptors for CO_2 Electroreduction to Methane on Transition-Metal Catalysts. *J. Phys. Chem. Lett.* **2012**, *3*, 251-258.

22. Manthiram, K.; Beberwyck, B. J.; Alivisatos, A. P. Enhanced Electrochemical Methanation of Carbon Dioxide with a Dispersible Nanoscale Copper Catalyst. *J. Am. Chem. Soc.* **2014**, *136*, 13319-13325.

23. Gattrell, M.; Gupta, N.; Co, A. A review of the aqueous electrochemical reduction of CO_2 to hydrocarbons at copper. *J. Electroanal. Chem.* **2006**, *594*, 1-19.

24. Castner, D. G.; Hinds, K.; Grainger, D. W. X-ray Photoelectron Spectroscopy Sulfur 2p Study of Organic Thiol and Disulfide Binding Interactions with Gold Surfaces. *Langmuir* **1996**, *12*, 5083-5086.